Line shape parameters of air-broadened 12CO2 transitions in the 2.0 μm region, with their temperature dependence

D. Mondelain, A. Campargue, H. Fleurbaey, S. Kassi, S. Vasilchenko

$^{12}CO_2$ transitions in the 2.0 µm region, with their temperature dependence

D. Mondelain*, A. Campargue, H. Fleurbaey, S. Kassi, S. Vasilchenko

Univ. Grenoble Alpes, CNRS, LIPhy, 38000 Grenoble, France

*Corresponding author: didier.mondelain@univ-grenoble-alpes.fr; LIPhy, Bat. E, 140 rue de la Physique, 38400 Saint-Martin d'Hères (France).

Key words

Line shape; carbon dioxide; temperature dependence; CRDS

Abstract

The 20013-00001 and 20012-00001 bands of $^{12}C^{16}O_2$ in the 2 µm region are used by many instruments on-board satellites and in ground-based networks to monitor the CO_2 column-averaged dry air mole fraction in the Earth's atmosphere. An accurate knowledge of the corresponding spectroscopic parameters and their temperature dependence is thus needed to map sources and sinks of carbon dioxide. In this work, we retrieve the line-shape parameters and their temperature dependence exponents/coefficients for the P(16) and P(28) transitions of the 20012-00001 band, and the R(24) and R(30) transitions of the 20013-00001 band. These parameters are obtained from a multi-spectrum fit procedure using a speed-dependent Nelkin-Ghatak profile including the line-mixing effect in its first-order approximation. High signal-to-noise spectra (quality factor between typically 3000 and 6000) are recorded at different conditions of pressure (from 50 to 750 Torr) and temperatures (from 245 to 330 K) for mixtures of CO_2 in air using a comb-assisted cavity ring down spectrometer with a temperature stabilized high finesse cavity. Air-broadening coefficients are measured with an estimated uncertainty better than 0.1% and absolute frequencies of the transitions are obtained with uncertainty better than 100 kHz. The determined line-shape parameters are consistent with previous values derived in the 1.6 µm region confirming the absence of significant vibrational dependence (except for the air-pressure shift coefficient). The retrieved parameters agree well with literature values by Fourier transform spectroscopy and classical molecular dynamic simulations. The parameters of the speed-dependent Voigt profiles provided by the HITRAN2020 database are mostly validated. The comparison to the CO_2 line parameters adopted for the OCO missions is discussed.

1. Introduction

The 20013-00001 and 20012-00001 bands of $^{12}CO_2$ in the 2 µm region have been the subject of several spectroscopic studies using Fourier transform spectroscopy (FTS) [1,2,3,4,5,6,7,8], laser diode absorption spectroscopy [9,10,11,12,13,14] and cavity ring down spectroscopy (CRDS) [15,16]. This interest is driven by the use of these bands (and the 1.6 µm bands) by instruments on-board satellites in GOSAT, GOSAT-2 (JAXA), OCO-2 (NASA), TanSat (CAS), and the upcoming MicroCarb (CNES) and CO2M (ESA) missions and in ground-based networks like TCCON [17] to monitor the CO_2 column-averaged dry air mole fraction in the Earth's atmosphere. Satellite missions are increasingly demanding in terms of high quality spectroscopic data. For example, the requirements of the CO2M mission lead to strong constraints on the accuracy of the spectroscopic parameters with an uncertainty on the air-broadening coefficients lower than 0.1% and better than 0.005 for their temperature dependence exponent (which is on the order of 0.7) [18]. Moreover, one of the conclusions of Oyafuso *et al.* [19] dedicated to the validation of 1.6 µm and 2.06 µm CO_2 absorption models for OCO-2 is that: "*The inclusion of measurements to the analysis from other laboratory techniques, such as Cavity Ringdown Spectroscopy, CRDS, (…) and Photoacoustic Spectroscopy (…) can offer extremely high signal to noise ratios and could potentially offer more stringent constraints on the line shape and line mixing.*". In addition, spectroscopic parameters with reduced uncertainty are valuable to test/evaluate the accuracy of *(i)* classical molecular dynamic simulations [20], *(ii)* the semi-empirical approach described in [21] and adopted in HITRAN2020 [22] and *(iii)* line shape calculations based on the modified complex Robert-Bonamy formalism [23,24]. Most of the above-mentioned experimental studies used a Voigt profile as line shape thus excluding speed-dependence, Dicke narrowing and line-mixing effects, the latter being particularly important for accurate remote sensing retrievals of atmospheric CO_2 [25,26]. The only exceptions are Refs. [1,15] where a speed-dependence Voigt (including line-mixing) and a speed-dependent Nelkin-Ghatak profile were adopted, respectively. These two studies will be used below for comparison to our line profile parameters.

The present work is part of the *Improved Spectroscopy for Carbon Dioxide, Oxygen, and Water Vapour Satellite Measurement* (ISOGG) project [27] funded by ESA and dedicated, in particular, to the improvement of the spectroscopic database of CO_2, and possibly interfering H_2O, in the 1.6 and 2.0 µm regions to meet the data product requirements for the CO2M mission [28]. Following our previous work in the 1.6 µm region [29], we undertake here a line profile study by CRDS in the 2.0 µm region for the P(16) and P(28) transitions, belonging to the 20012-00001 band, and the R(24) and R(30) transitions, in the 20013-00001 band, of $^{12}CO_2$. To achieve the highly demanding level of accuracy, our CRDS spectrometer is linked to a frequency comb referenced to a rubidium clock. In addition, a recently developed temperature regulated high finesse cavity (TR-HFC) is combined to the CRDS spectrometer to study the temperature dependence of the line profile parameters.

In the next Part 2, the experimental setup is described together with the procedure adopted to record the spectra of CO_2 in air. The line profile analysis is detailed in Part 3, then the retrieved parameters are compared with datasets available in the literature and discussed (Part 4). Finally, concluding remarks and perspectives close our report (Part 5).

2. Experimental setup and spectra recording

2.1. Experimental setup

The comb-referenced cavity ring down spectrometer used here has been described in [29,30,31]. In these previous works, the light source was a DFB laser diode (narrowed by an optical feed-back from a high finesse V-shape cavity in [29]), while here, an extended cavity diode laser (ECDL) (New Focus; Model TLB 6736) covering the 1975-2075 nm range was used. In addition, a recently developed temperature stabilized high finesse cavity (TS-HFC), described in [32,33], replaces the

standard CRDS cell used at room temperature. The TS-HFC used in this work, named V2 in [33], allows controlling the temperature of the gas sample between 240 and 330 K with an accuracy and homogeneity better than 0.1 K. The temperature is measured thanks to four Pt100 temperature sensors placed at the surface of a inner copper tube [33] put between the two high reflectivity mirrors [33] (from Layertec, with a reflection coefficient *R*>99.99% over the 1950-2250 nm range) corresponding to the 45.5 cm long CRDS cell. Most of the ECDL light (~90%) is sent into the TS-HFC where the output cavity mirror, mounted on a PZT tube, allows for periodic resonances between the laser light and a cavity mode thanks to a voltage triangular ramp applied on the PZT. The resonance leads to a build-up signal on the detector (InGaAs PIN photodiode; G12183 series from Hamamatsu) which triggers the interruption of the photons injection with the help of an acousto-optic modulator (AOM) when the detector signal exceeds a user-defined voltage threshold. A ring down (RD) event is then obtained at frequency ν and fitted to derive the ring down time, $\tau(\nu)$, and the extinction coefficient, $\alpha(\nu)$, given by:

$$\alpha(\nu) = \frac{n}{c\tau(\nu)} - \frac{1-R(\nu)}{L_{cav}} \quad (1)$$

where *c* is the speed of light, *n* is the refractive index of the absorbing gas, R(v) is the reflectivity of the mirrors and L_{cav} is the cavity length. Typical RD times of the evacuated cell are τ ~ 55 µs at 4875 cm^{-1} and ~48 µs at 4953 cm^{-1} for a cavity length of ~45 cm.

An absolute frequency of the laser is associated to each RD event by measuring the beat note (BN) frequency between a part (~5%) of the light emitted by the laser source and the closest tooth of a frequency comb (FC) (Model FC 1500-250 WG from Menlo Systems) (see [29] for the details). The BN signal is obtained with a fast extended InGaAs photodiode (Model UPD-3N-IR2-P from Alphalas; bandwidth > 400 MHz). The repetition rate, f_{rep}= 250 MHz, and the carrier-envelop offset, f_{CEO}=±20 MHz, of the FC are referenced to a 10 MHz rubidium frequency standard (Model PRS 10 from SRS) which is phase-locked to a GPS timing receiver. This is also the case for the direct digital synthesizer (DDS) which generates the sinusoidal wave applied to the AOM and for the fast BN acquisition board. The accurate knowledge of these frequencies together with the determination of the tooth number with a commercial wavelength meter (HighFinesse WS7-60 IR-II) leads to the measurement of the laser frequency with an uncertainty of ~200 kHz (mainly limited by the ECDL jitter) for a BN measurement rate of ~400 Hz.

2.2. Acquisition procedure

Each spectrum is recorded by applying a voltage ramp between -3 V and +3 V, through the *Frequency modulation input* of the laser controller, to the piezoelectric transducer (PZT) moving the arm of the tuning mirror of the external-cavity. A mode hop-free tuning is then obtained over ~1 cm^{-1}. The voltage ramps are generated by a home-made low-noise voltage generator with typical voltage steps of 0.033V (for the 500 and 750 Torr spectra) or 0.017V (for the 50, 100 and 250 Torr spectra) leading to a mean spectral sampling of 5×10^{-3} and 2.5×10^{-3} cm^{-1}, respectively. At each spectral step, the frequency of the ECDL is smoothly stabilized with the *Current modulation input* of the controller to keep the measured BN frequency constant. Two hundred RD events are acquired at rates of 100 to 200 RD/s, by applying the tracking procedure described in [29], before moving on to the next spectral step. The average time for the recording of one line profile is typically 15 to 20 min. An *a posteriori* software allows averaging, for each spectral step, the RD times and associated absolute frequencies derived from the BN frequencies.

2.3. Spectra recording

Table 1 lists the transitions recorded in this work and the temperature and pressure conditions of the recordings. For each temperature, a series of spectra is acquired for 5 total pressures applying the acquisition procedure described above. For each pressure value, three spectra are generally recorded successively allowing evaluating CO_2 mixing ratio changes with time (see below).

Transitions	**(20012) ← (00001)** P(16) and P(28) **(20013) ← (00001)** R(24) and R(30)
Temperature (K)	245, 260, 274, 296, 330
Pressure (Torr)	50, 100, 250, 500, 750

Table 1. *Summary of the transitions studied in this work and temperature and pressure values of the recordings.*

Because of the different intensities of the studied bands (the 20012-00001 band is about 4 times stronger than the 20013-00001 band), two gas mixtures of CO_2 in air (Ar : ~1 Mol-% ; O_2 : ~20.95 Mol-% ; N_2 : ~78.05 Mol-%) are used. The stated sample CO_2 mixing ratios are 6.013±0.060 Mol-ppm for the 20012-00001 band and 40.10±0.24 Mol-ppm for the 20013-00001 band.

As an example, we present in **Figure 1**, the series of recordings of the R(24) transition of the 20013-00001 band at 245 K. Residuals at the noise level (which is between 1×10^{-10} and 2×10^{-10} cm^{-1}) are achieved for all the pressure values, using the multi-spectrum fit procedure presented below. This leads to quality factors (*QF*) between 3700 and 5800 in this case (*QF* being defined as the ratio of the absorption at the peak to the *rms* of the residuals).

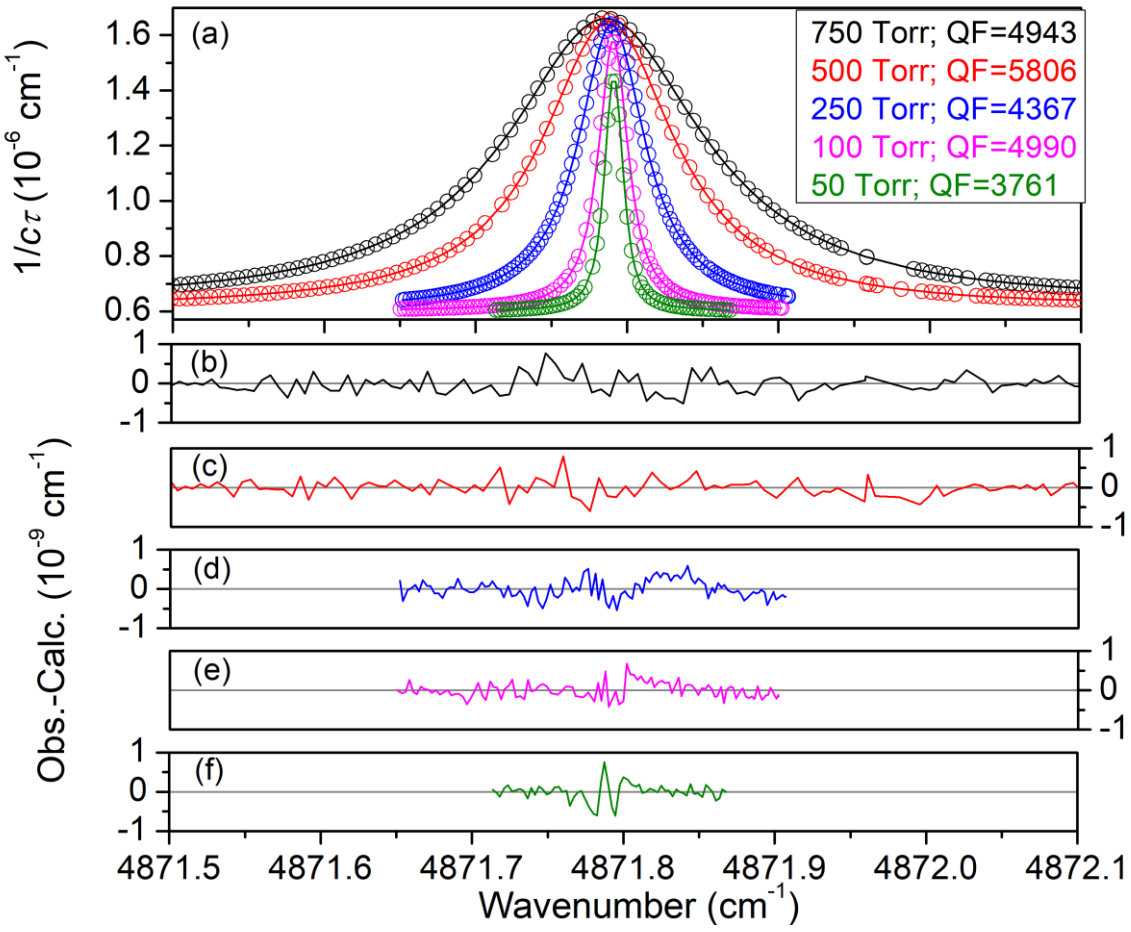

Figure 1.

Panel (a): CRDS spectra at 245 K of the R(24) transition of the 20013 - 00001 band recorded at several pressures with the mixture of 40 ppm of CO_2 in air.

Panels (b) to (f): Corresponding (exp.-fit) residuals obtained after the multi-spectrum fit procedure for 750, 500, 250, 100 and 50 Torr total pressure. Residuals at the experimental noise level are achieved leading to quality factor (QF) between 3761 and 5806.

3. Line profile analysis

3.1. Spectra fit

In a first step, each spectrum is fitted independently with a speed-dependent Nelkin-Ghatak profile (SDNGP) [34] including the line mixing (LM) effect in its first-order approximation [35] to derive the corresponding CO_2 mixing ratio, $X_{CO_2\_Fit}$, by fixing the transition intensity to its HITRAN2020 value [22]. Due to different processes in particular adsorption on the inner copper tube, the CO_2 mixing ratio is not strictly constant during the recordings. From the successive recordings performed at a given pressure, the variation rate, *r*, is obtained for each (*P, T*) condition, by fitting the linear change of X_{CO_2} with time. The mixing ratio was found to vary slightly for the four lowest temperatures: the relative X_{CO_2} variation is within ±1%, over a spectral interval corresponding to 6 times the FWHM of the line profile, for 95.3% of the spectra and within ±2% for all the spectra. Nevertheless, for the highest temperature (330 K), and the lowest concentration (*i.e.* 6 ppm CO_2 in air mixture) variations of several percents are observed.

To avoid a bias on the line profile due to these mixing ratio variations with time, we correct all the spectra in the following way:

$$\frac{1}{c\tau_{corr}(\nu)} = \left[\left(\frac{1}{c\tau(\nu)} - \frac{1}{c\tau_0(\nu)}\right).A + \frac{1}{c\tau_0(\nu)}\right] \quad (2)$$

where τ_0 is the RD time for the empty cavity and $A = \frac{X_{CO_2\_Fit}}{X_{CO_2\_Fit}+r(t-t_c)}$ with *t* and t_c the fractional times at the frequency ν and at the line center, respectively. The slope *r* is obtained by fitting the linear change of X_{CO_2} with time for a given temperature and pressure. This correction procedure was validated by the observed decrease of the residuals of the multi-spectrum fit of the spectra at 330 K described just below: residuals at the noise level could be achieved whereas systematic structures are observed for the uncorrected spectra.

For a given transition recorded at several pressures, a multi-spectrum fit procedure is applied at each temperature to the corrected spectra using the *Multi-spectrum Analysis Tool for Spectroscopy (MATS)* fitting program developed at NIST [36]. During this procedure a SDNG profile [34] is adopted including line mixing in its first-order approximation [35]. This profile takes into account the Doppler effect, the collision-induced velocity changes, quantified by the velocity changing collision rate (in cm^{-1}), ν_{VC}, the collisional broadening and shift for which a quadratic law is used for the speed dependence.

In this multi-spectrum fit procedure (**Figure 1**), the wavenumber of the spectral line at zero pressure, ν_0, the line-broadening and pressure-shift coefficients γ_0 (in $cm^{-1}atm^{-1}$) and δ_0 (in $cm^{-1}atm^{-1}$), their speed dependence components γ_2 (in $cm^{-1}atm^{-1}$) and δ_2 (in $cm^{-1}atm^{-1}$), respectively, the Dicke narrowing parameter β (in $cm^{-1}atm^{-1}$) and the first-order line-mixing coefficient ζ (in atm^{-1}) are globally fitted for each temperature. The Doppler width is fixed to its value calculated at the measured temperature averaged over the temperature sensors. The intensity of each transition is fixed to its HITRAN2020 value and X_{CO_2}, corrected from the variations, is fitted independently for each spectrum together with the linear baseline. All the spectra recorded for the same temperature and pressure conditions are included in the multi-spectrum fit procedure.

Note that during the fit procedure, the absorption due to the weak CO_2 lines in the neighbourhood of the fitted transition is taken into account by the *MATS* program based on the HITRAN2020 database [22] using a Voigt profile.

In the end, a set of 6 parameters (ν_0, γ_0, γ_2, δ_0, β, ζ) is retrieved for each transition and at each temperature (δ_2 is fixed to 0 to avoid over fitting the spectra). The complete set of obtained parameter values is given as *Supplementary Material*.

3.2. Temperature dependence of the spectroscopic parameters

The values retrieved at each temperature for a given parameter are then fitted with a power law of the form: $A(T) = A(T_{ref})\left({T_{ref}}/{T}\right)^{n_A}$ where T_{ref} = 296 K, $A(T)$ corresponds to either γ_0, γ_2, β or ζ and n_A is the corresponding temperature dependence exponent. For the pressure shift, δ_0, the linear dependence $\delta_0(T) = \delta_0(T_{ref}) + \delta_0'(T - T_{ref})$ is adopted. **Figure 2** illustrates the results of the fits for the four transitions studied. For the fit, the data points are weighted by the inverse of the squared uncertainty estimated as discussed below. The values of the line profile parameters at T_{ref} and their temperature dependence exponents/coefficients are reported in **Table 2** with their uncertainties corresponding to the fit error.

Note that in the *MATS* program, the fit output corresponds to $a_w = \frac{\gamma_2(T)}{\gamma_0(T_{ref})}$ so that, by plotting $a_w(T)$ *versus* T_{ref}/T and fitting these data points with a function of the form $y = ax^b$, we obtain $a_w(T_{ref}) = \gamma_2(T_{ref})/\gamma_0(T_{ref})$ and n_{γ_2}.

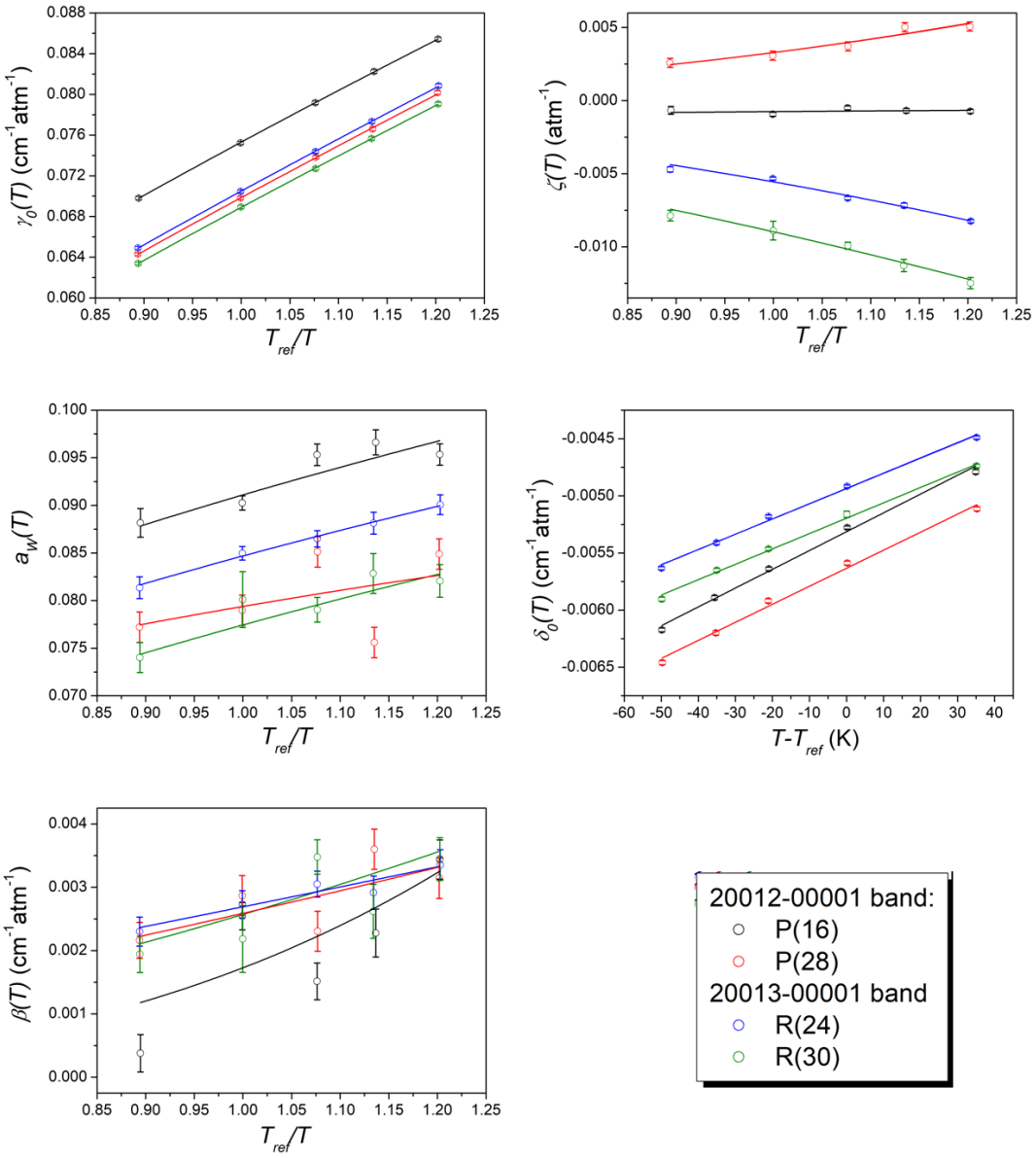

Figure 2. *Retrieved parameters at each temperature for the R(24) and R(30) transitions of the 20013-00001 band and for the P(16) and P(28) transitions of the 20012-00001 band of $^{12}CO_2$. The parameters γ_0, β, a_w, ζ are fitted with a function of the form $y= ax^b$ to determine their value at T_{ref} and the temperature dependence exponent. The δ_0 parameter is fitted with a linear function which provides its value at T_{ref} and the temperature dependence coefficient.*

	ν_0	γ_0	$n_{\gamma 0}$	δ_0	δ'	β	n_β	a_w	$n_{\gamma 2}$	ζ	n_ζ
	cm^{-1}	$cm^{-1}atm^{-1}$		$cm^{-1}atm^{-1}$	$cm^{-1}atm^{-1}K^{-1}$	$cm^{-1}atm^{-1}$				atm^{-1}	
R(24)$^+$	4871.791689(3)	0.07049(2)	0.738(3)	-0.00493(2)	0.0000134(5)	0.00269(7)	1.2(2)	0.0847(2)	0.33(2)	-0.00556(14)	2.1(2)
R(30)$^+$	4875.748723(3)	0.06890(2)	0.744(3)	-0.00520(1)	0.0000135(4)	0.00257(27)	1.8(8)	0.0774(7)	0.36(8)	-0.00897(17)	1.7(2)
P(16)$^\#$	4964.465159(3)	0.07531(2)	0.684(2)	-0.00531(2)	0.0000165(7)	0.00173(47)	3.4(21)	0.0911(8)	0.33(9)	-0.00075(12)	-0.7(14)
P(28)$^\#$	4953.206614(3)	0.06986(5)	0.741(6)	-0.00563(2)	0.0000158(7)	0.00259(24)	1.4(8)	0.0794(23)	0.22(24)	0.00327(20)	2.6(5)

***Table 2**. Spectroscopic parameters of the transitions of the 20012-00001 (marked with $^\#$) and 20013-00001 (marked with $^+$) bands of $^{12}CO_2$. A SDNG profile is used in the multi-spectrum fit procedure. One-sigma uncertainties are given in parenthesis in the unit of the last digit. Here, a_w corresponds to γ_2/γ_0.*

3.3. Estimated error budget

The error budget for the retrieved spectroscopic parameters at temperature *T* is estimated exactly as described in [29]. For type-A uncertainty, we use typical noise conditions (20 kHz or σ_x= 6×10^{-3}% of the Doppler FWHM on the x-axis and 2×10^{-10} cm^{-1} or σ_y= 0.04% of the maximum absorption on the y-axis) to simulate 100 spectra with random noise. We find, as in [29], that the uncertainty given by the *MATS* program corresponds to the error derived from the simulations, showing that the impact of the correlation between the parameters is small thanks to the low noise level on the two axis. Hence, the type-A uncertainties correspond to the fit errors.

Type-B uncertainties are estimated, as in [29], by taking a bias of 0.1% for the total pressure, corresponding mostly to the uncertainty of the pressure gauge, and a bias of 0.1 K for the temperature. This 0.1 K value accounts for both the uncertainty on the measured temperature value and the inhomogeneity of the sounded gas temperature [33]. These evaluations are done for all the transitions and temperatures. As $X_{CO_2}$is fitted for each spectrum, it is not considered here as a source of bias.

In the end, the final uncertainty is obtained as the square root of the quadratic sum of the type-A and type-B errors. These 1σ-final uncertainties are reported at temperature *T* for each parameter in the *Supplementary Material*. The 2σ-final uncertainties are also included in **Figure 2**. From the comparison of the error bars, plotted on this figure, to the deviation from the fitted curves, we conclude that uncertainties seem to be well estimated for γ_0 and ζ for all the transitions and for a_w for the R(24) and R(30) transitions. For this latter parameter, a slight underestimation is visible for the P(16) transition whereas a clear underestimation appears for the P(28) transition. Finally, uncertainties are clearly underestimated (by a factor 2 to 3) for the δ_0 and β parameters (except for the R(24) transition for this latter). Note that for a given transition, the v_0 values retrieved at the different temperatures are nearly in agreement within their 2σ-final uncertainties. These uncertainties are similar to what was achieved in the 1.6 µm region [29] where a maximum difference of 27 kHz was observed compared to the Lamb-dip measurements with sub-kHz uncertainties [37]. A (conservative) uncertainty of 100 kHz (or 3×10^{-6} cm^{-1}) is adopted here for the absolute zero-pressure wavenumbers in the 2.0 µm region (**Table 2**). Contrary to the 1.6 µm region, no highly accurate position frequencies are available for comparison in the 2 µm region. In Benner2016 [1], positions are reported with an uncertainty of ~1×10^{-6} cm^{-1} but this value corresponds to the internal statistical error obtained from the multi-spectrum fit and doesn't include systematic errors (especially the frequency axis calibration). Hence, we observe that Benner2016 absolute positions are higher by $+21\times10^{-5}$ cm^{-1} compared to our positions for the R(24) and R(30) transitions of the 20013-00001 band. For the same transitions, HITRAN2020 values are smaller by -6×10^{-5} cm^{-1} compared to our measurements. A difference of -11×10^{-5} cm^{-1} is found for the P(16) and P(28) transitions of the 20012-00001 band when comparing HITRAN2020 values to ours.

4. Discussion

The line-shape parameters and their temperature dependence retrieved in this work are compared with the most relevant literature data. We mainly select the following datasets:

- FTS measurements from Benner *et al.* [1], called hereafter Benner2016, which constitute the reference dataset for the CO_2 line-shape parameters in the 2.06 µm band for OCO missions [38] and for which speed-dependent Voigt (SDV) profiles with line mixing are used,
- Classical molecular dynamic simulations reported in Nguyen *et al.* [20], called hereafter Nguyen2020, which are used to complete the HITRAN database with non-Voigt line shape parameters,
- The latest version of the HITRAN database [22], HITRAN2020, where parameters for SDV profile and the line-mixing are provided,

- A previous study by frequency-stabilized cavity ring-down spectroscopy [15] at NIST and at the Nicolaus Copernicus University of Torun, called hereafter Bui2014, where a sophisticated partially correlated speed-dependent Nelkin-Ghatak (pCSDNG) is adopted for the multi-spectrum fit analysis (without line-mixing) of the R(24) and R(30) transitions belonging to the 20013-00001 band.

4.1. The air-broadening coefficients and their temperature dependence exponents

The retrieved air-broadening coefficients at 296 K, $\gamma_0(T_{ref})$ are plotted on **Figure 3** together with those of the four selected datasets mentioned above and two additional studies: one by FTS [6] (Toth2008) and the other one by laser diode spectroscopy [9] (Joly2009). For the R-branch of the 20013-00001 band, we observe that Bui2014 values for the R(24) and R(30) transitions are overestimated by ~5% compared to all the other measurements which are in agreement at the percent level. The only other exception is the R(26)-R(34) dataset of Joly *et al*. [9] for which the *m*-dependence differs from other datasets (with $m = -J$ for the P-branch and $J+1$ for the R-branch). For the P-branch of the 20012-00001 band, the agreement is also within the percent level for the three datasets plotted. In both bands our values confirm the sub-percent level of accuracy estimated for the HITRAN2020 values.

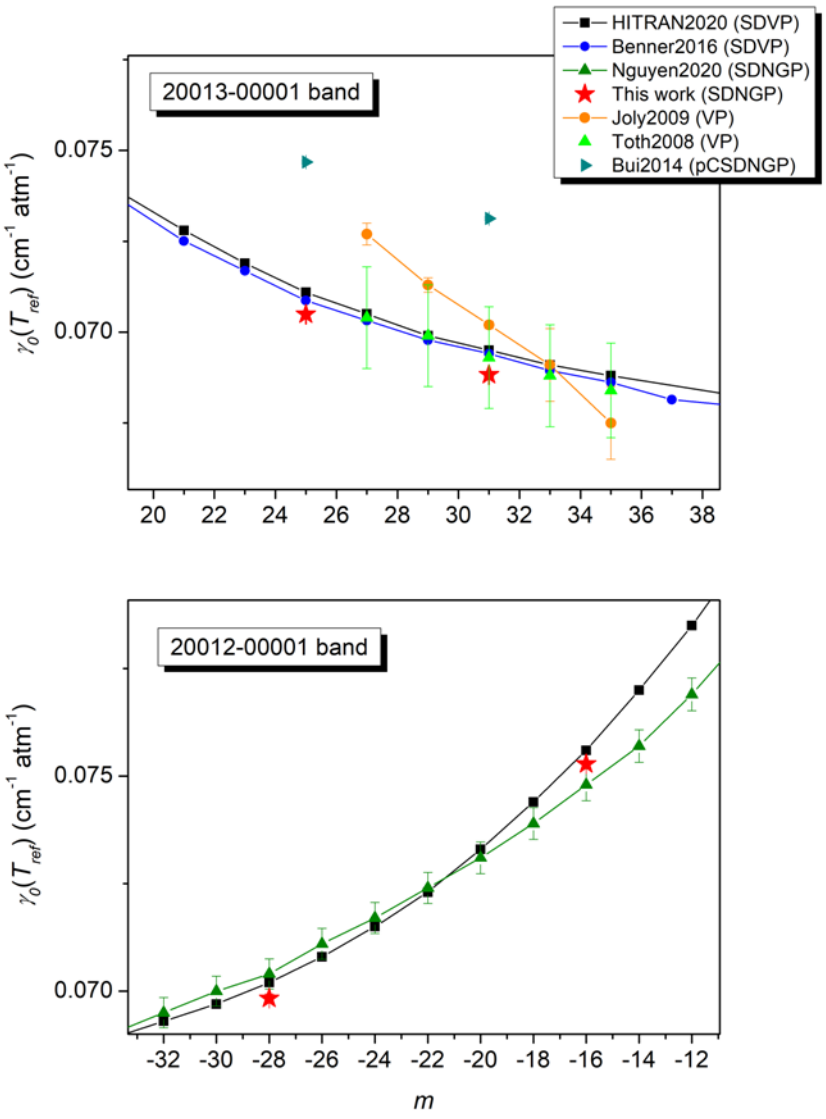

Figure 3. *Air-broadening coefficients at T_{ref}=296 K reported in Nguyen2020 [20] and HITRAN2020 [22] for the R-branch of the 20013-00001 band (upper panel) and the P-branch of the 20012-00001 band (lower panel) and in*

Benner2016 [1], Bui2014 [15], Joly2009 [10] and Toth2008 [6] for the former one. Here m= -J for the P-branch and J+1 for the R-branch).

To look more closely at the agreement between our retrieved values and Benner's dataset, their ratios to the HITRAN2020 values are plotted in **Figure 4**. For the R(24) and R(30) transitions, values of Benner2016 are 0.5 and 0.8% higher than ours, respectively. As the vibrational dependence is expected to be very weak, we have also included on the figure the air-broadening coefficients retrieved in [29,39,42] for the 1.6 µm region. In Ref. [42] (Ghysels2017, hereafter), the line-shape parameters of the R(16) transition in the 30013-00001 band (near 1.6 µm) were derived by the FS-CRDS. At first glance, we can observe that the ratios show a similar evolution with $|m|$ (decrease for $|m|\leq 17$ and almost constant value for $|m|>17$), but with different amplitudes. Our values obtained for the R(24) and R(30) transitions look consistent with our previous data of the R(6), R(12), R(16), R(18) and R(20) transitions near 1.6 µm. Another important observation is the systematic higher ratios for the P-branch compared to the R-branch which are observed for the three datasets of **Figure 4**. This asymmetry between the two branches, already mentioned in Ref. [28], cannot be reproduced by the single empirical formula *versus* $|m|$ used in the HITRAN2020 for both branches. It leads to errors at the ~0.5% level.

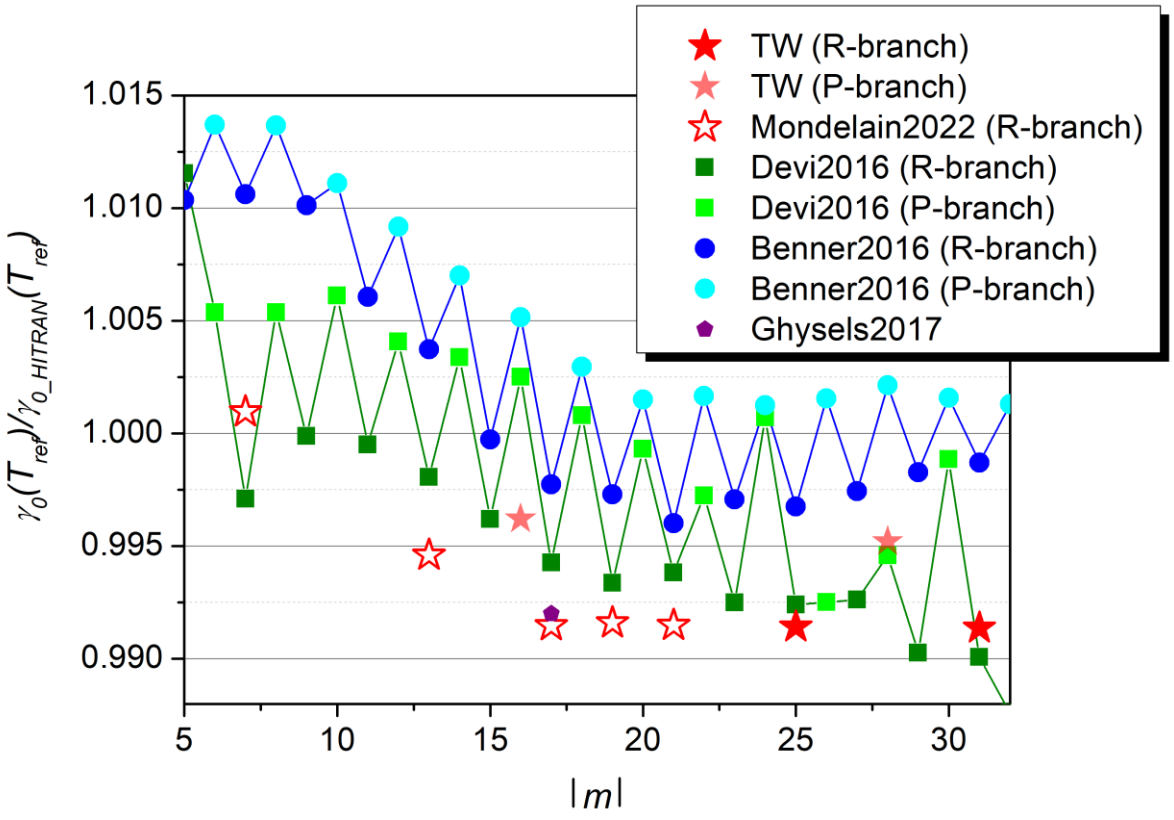

Figure 4. *Ratios of the air-broadening coefficients at T_{ref}=296 K reported in [1] (Benner2016), and in this work (TW), for the 2.0 µm region (corresponding to the 20013-00001 and 20012-00001 bands), and in [29] (Mondelain2022), [42] (Ghysels2017) and [39] (Devi2016) for the 1.6 µm region (corresponding to the 30013-00001 band), to the HITRAN2020 values [22].*

The temperature dependence exponents of the air-broadening coefficients, n_{γ_0}, retrieved in this work (and in our previous work at 1.6 µm [29]) are compared with the values reported in Benner2016, HITRAN2020, Ghysels2017 and Joly2009. If we except data of Joly2009, which are clearly underestimated, the overall agreement between the different datasets is good. Maximum

absolute differences of 0.02 of HITRAN2020 values compared to our CRDS measurements are observed. This is largely within the adopted error bars (~0.035) of HITRAN values. Benner's values are systematically higher than ours with differences of ~0.02 and ~0.03 for the R(24) and R(30) transitions of the 20013-00001 band. For the latter transition it results in differences above the percent level on $\gamma_0(T)$ for T<275 K.

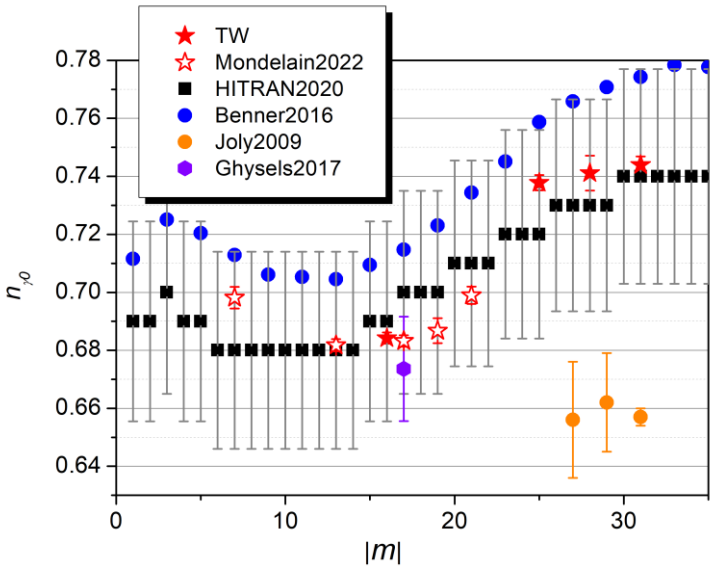

Figure 5. *Temperature dependence exponents of the air-broadening coefficients reported for the 20012-00001 and 20013-00001 bands in this work (red full stars), in HITRAN2020 (black squares), in Benner2016 (blue circles) and in Joly2009 (orange circles), for the 30013-00001 band in Mondelain2022 (red open stars) and in Ghysels2017 (violet hexagons).*

4.2. The air-pressure shift coefficients

Previous air-pressure shift data are very scarce in the 2 µm spectral region. As explained in [21], HITRAN2020 values are obtained using the Hartmann's approach described in [40]. This approach reproduces very well the data of Toth *et al.* (Toth2007) hereafter [4] (see Fig. 1 of [40]). At this point, it is necessary to discuss the impact of the chosen line profile on the derived value of the air-pressure shift coefficients. For comparison purpose, we have analyzed our data with a Voigt profile (VP) *excluding* line-mixing effect (as adopted by Toth *et al.* in [4]). **Figure 6** compares the obtained VP air-pressure shift coefficients to our best values obtained with a SDNG profile including the line-mixing effect. The impact of the line profile on the retrieved values is clearly apparent. The VP values are in good agreement with Toth2007 and HITRAN2020 data except for the P(28) transition for which a smaller value is observed for these two data sets. Note that our data points (obtained with the Voigt profile) are largely within the 0.01 $cm^{-1}atm^{-1}$ error bars of the HITRAN2020 values.

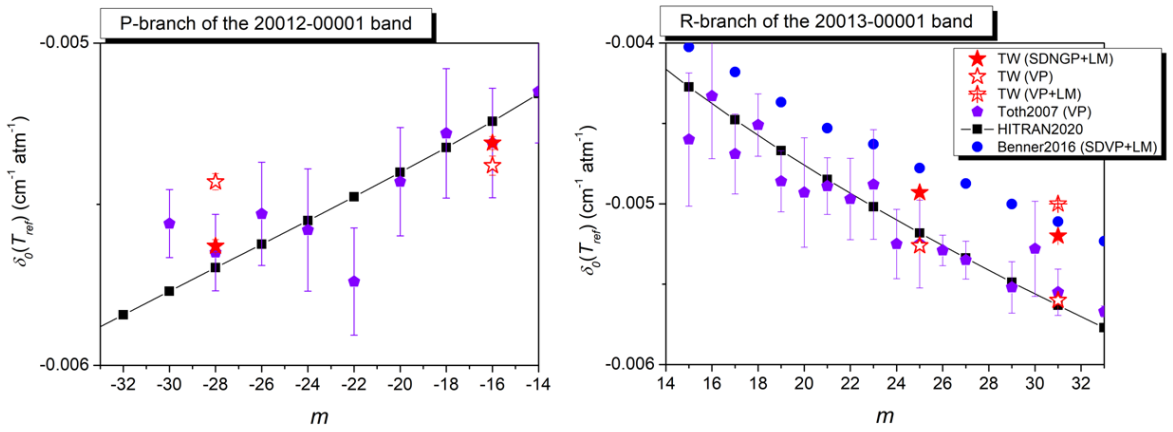

Figure 6. *Air-pressure shift coefficients reported in this work for a SDNG profile + LM (red filled stars) and a Voigt profile (red open stars), in HITRAN2020 (black squares), in Toth2007 (dark cyan hexagons) and in Benner2016 (blue circles) for the P-branch of the 20012-00001 band (left panel) and for the R-branch of the 20013-00001 band (right panel). Note the factor of 2 between the y-scale of the two panels.*

4.3. The speed-dependent parameters and their temperature dependence

The values of the speed-dependence parameter for the air-broadening, $a_w(T_{ref}) = \frac{\gamma_2(T_{ref})}{\gamma_0(T_{ref})}$, retrieved in this work and in [29] for the 1.6 µm region, are reported on **Figure 7** and compared to the few previous datasets available in the literature. Our two datasets at 1.6 µm and 2.0 µm are consistent with each other showing that the vibrational dependence for a_w is very weak. This is confirmed by the very good agreement observed with values obtained by Wilzewski *et al.* for the ν_3 band of $^{12}CO_2$ in nitrogen using FTS [41] and by Ghysels *et al.* for the R(16) transition in the 30013-00001 band using the FS-CRDS technique [42]. The agreement is also very good with rCMDS calculations of Nguyen2020 where the same SDNG profile was adopted. HITRAN2020 values are derived from rCMDS calculations but with a SDV profile using a Padé approximant [21]. As discussed in [21], the larger a_w HITRAN2020 values are due to the fact that in the SDV profile, the Dicke narrowing effect is not taken into account. The Benner2016 [1] and Devi2016 [39] FTS values included in **Figure 7** are significantly higher and show a different *m* dependence, possibly due to the fact that in these two studies, the speed dependence was assumed independent of the perturber gas and of the temperature. As shown in the lower panel of **Figure 7**, this latter assumption is not validated by our measurements: in agreement to the experimental data of [41] and rCMDS calculations of [20], we observe that the temperature dependence coefficient n_{γ_2} is different from zero.

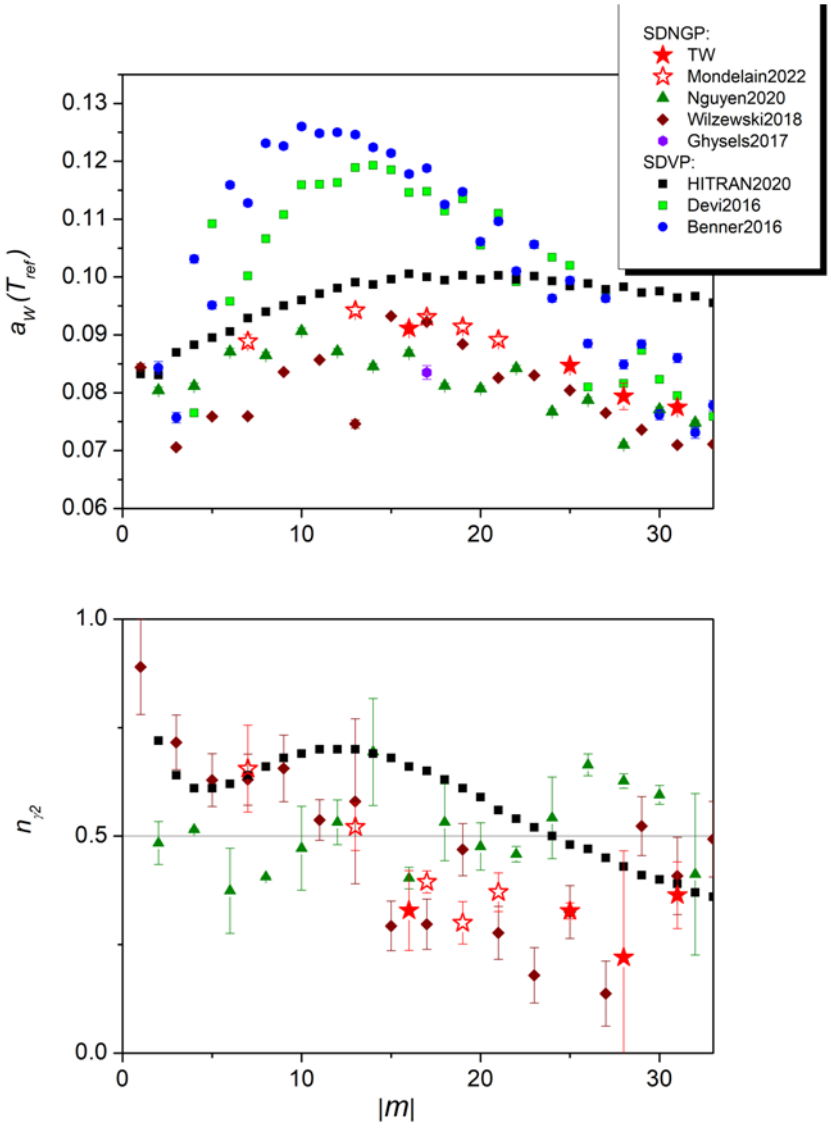

Figure 7. *The* $a_w(T_{ref}) = \frac{\gamma_2(T_{ref})}{\gamma_0(T_{ref})}$ *parameters (Upper panel) and their temperature dependence exponent (Lower panel) obtained in this work compared to Nguyen2020 [20], Wilzewski2018 [41], Ghysels2017 [42], Devi2016 [39], Benner2016 [1] and HITRAN2020 [22].*

4.4. The Dicke narrowing parameters

Figure 8 shows that the Dicke narrowing parameters, β, found in this work and the values derived in the 1.6 µm region [29] are mostly constant with values between 2×10^{-3} and 2.5×10^{-3} $cm^{-1}atm^{-1}$ (excluding one outlier for P(16)). This level of consistency is satisfactory taking into account the quite large error bars due to the small values of β (typically a factor 2 to 3 smaller than γ_2). These experimental data are consistent with the rCMDS calculations [20] and to a lesser extent to the experimental data of [41] for the ν_3 band reported with larger uncertainties. Note that all of these datasets adopt the same SDNG profile, which is important as the β parameter is strongly dependent of the line shape model. On the same figure, the temperature dependence exponents are also plotted showing a satisfactory agreement taking into account the large error bars.

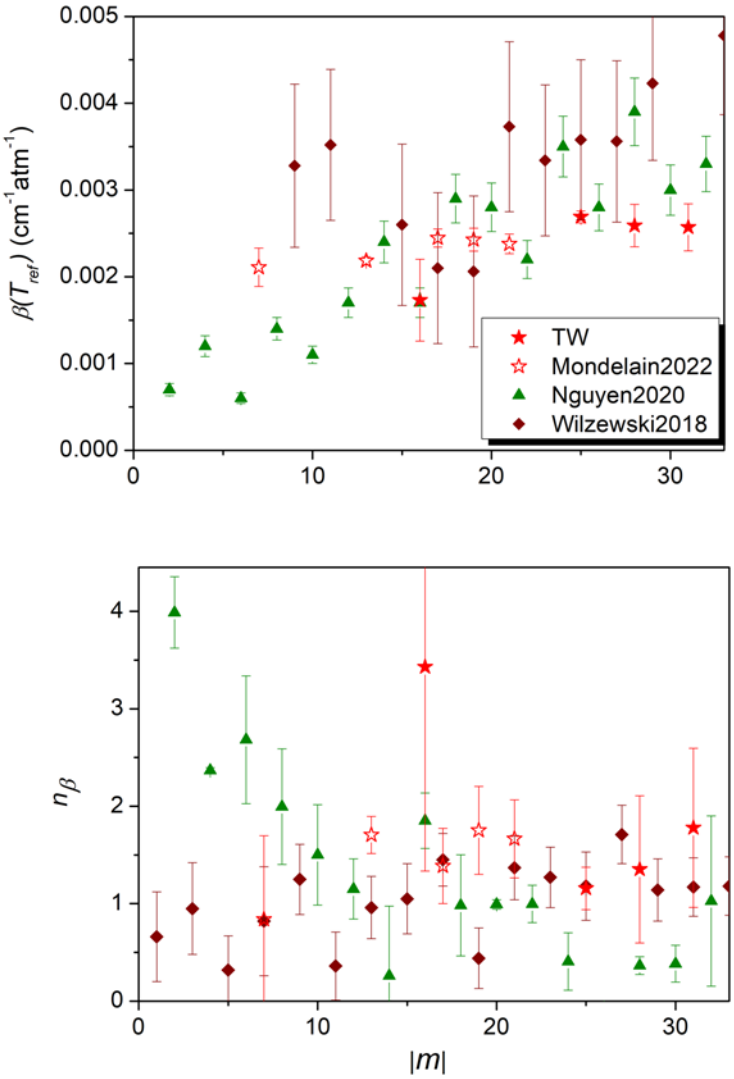

Figure 8. *Dicke narrowing parameters, β, (Upper panel) and their temperature dependence exponent (Lower panel) derived in this work and reported in Mondelain2022 [29], Nguyen2020 [20] and Wilzewski2018 [41] versus the absolute value of m.*

4.5. The line-mixing parameters

First order line-mixing parameters are presented on **Figure 9**. A very good agreement is noticed between our 2.0 and 1.6 µm data in the R-branch and the values of Wilzewski *et al.* in the ν_3 band [41]. In the P-branch, a very similar agreement is noted for the P(16) line, whereas an unexplained larger difference is observed for the P(28) line. The same behavior is observed in the P-branch when comparing our data with rCMDS calculations (for which no vibrational dependence is considered) [20]. A satisfactory agreement is achieved with HITRAN2020 values which are obtained from the off-diagonal relaxation matrix elements, W_{ij}, [21] calculated using the Energy-Corrected Sudden (ECS) approximation described in Lamouroux *et al.* [43]. In this theory the interaction between every line in a given band with every other line in that band is considered. This is not the case for the W_{ij} elements reported in Benner2016 (and in Devi2016) for which only the interaction with the closest neighbor is taken into account. The shortcomings of this (incomplete) approach are underlined in [19] and are clearly visible on **Figure 9**, in particular for the *R(J)* lines with *J* values larger than 20. Note that we

use Eq. IV.24 of [44] and Eq. 7 of [45] to convert the W_{ij} elements into the first-order line-mixing parameters plotted on **Figure 9**.

The temperature dependence exponents of the line-mixing parameter are displayed on the lower panel of **Figure 9.** The agreement between our new data points for the R(24) and R(30) transitions and the ν_3 band data [41] is very good. For the P-branch, the agreement is less satisfactory but remains between the 2σ-error bars of the reported exponents. In agreement with rCMDS calculations [20], the CRDS and FTS datasets show a rapid variation with m near m= ±15 which does not appear in the HITRAN2020 database and in the Benner2016 data. In fact, to simplify the calculations with HAPI [46], the HITRAN2020 values are either $n_\zeta = 0.41$ for $|m| \leq 16$ or $n_\zeta = 1.6$ for $|m| > 16$ [21].

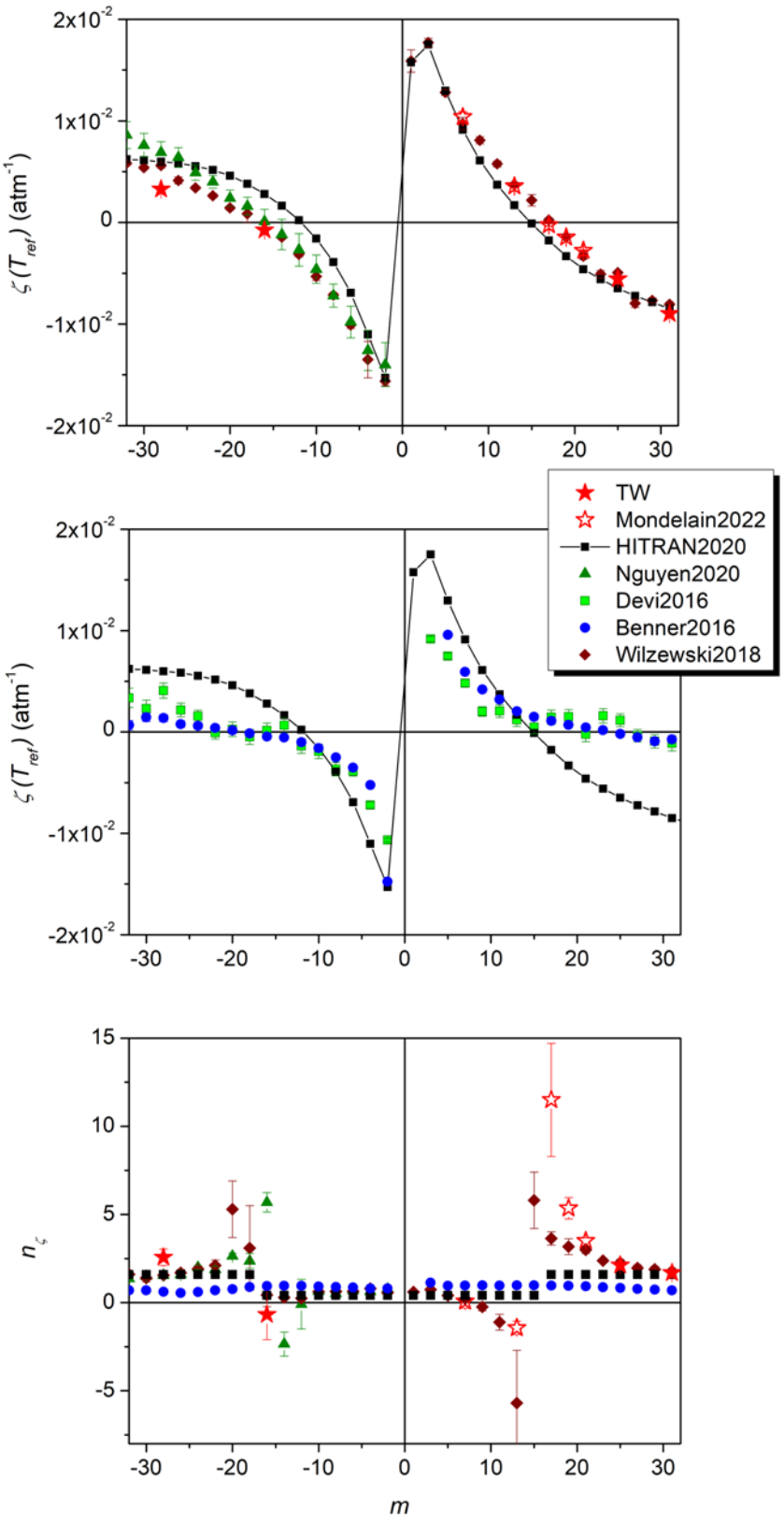

Figure 9. *Plot of the line-mixing parameters, in the first order approximation, ζ, reported in this work, Mondelain2022 [29], Nguyen2020 [20], Wilzewski2018 [41], HITRAN2020 [22] (Upper panel) and Devi2016 [39], Benner2016 [1] (Middle panel) and their temperature dependence exponent (Lower panel).*

5. Conclusion

A CRDS spectrometer, referenced to a frequency comb, allows recording spectra with S/N between typically 3000 and 6000 and achieving accurate frequency axis. In addition, a temperature regulated high finesse cavity ensures knowledge of the gas temperature better than 0.1 K. With this setup, series of CO_2 in air spectra are acquired in different pressure (50 to 750 Torr) and temperature (245 to 330 K) conditions for the P(16) and P(28) transitions of the 20012-00001 band, and the R(24) and R(30) transitions of the 20013-00001 band. Thanks to a multi-spectrum fit procedure adopting a speed-dependent Nelkin-Ghatak profile including the line-mixing effect with the first-order approximation, the different line-shape parameters and their temperature dependence exponents/coefficients are retrieved. Reduced uncertainties are obtained, particularly for the air-broadening coefficients (estimated uncertainty <0.1%) and their temperature dependence exponents (estimated absolute uncertainty <0.005) which are two crucial parameters to fulfill the drastic requirements of the upcoming satellite instruments. A very good agreement is observed for the different parameters between the new values obtained in this work and the data reported previously in [29] in the 1.6 µm region confirming the (very) weak vibrational dependence. A very satisfactory agreement with the FTS data of Ref. [41] and with rCMDS calculations of [20] is also noticed. Some deficiencies/limits of the line list provided by Benner *et al.* [1], adopted for the OCO missions, are evidenced. Finally, although more accurate, our results validate the parameters given in the HITRAN2020 database for speed-dependent Voigt profiles for the studied bands. The importance of the line-shape profile for comparison purposes is also underlined in the case of the air-pressure shift determination.

Altogether, the line profile of seven R lines and two P lines were investigated in the present work and in our preceding study in the 1.6 µm range [29]. The systematic difference of about 0.5% of the air pressure-broadening between the P- and R- branches, which is clearly observed in the FTS values of Benner2016 and Devi2016, seems to be confirmed by the overall set of CRDS values (see **Fig. 4**). It represents a large part of the uncertainties reported in HITRAN2020 which considers a universal law in $|m|$. The physical origin of these differences, between branches deserves to be investigated.

Acknowledgements

This work is funded by the European Space Agency (ESA) through the contract No. 4000132228/20/I-NS with Deutsches Zentrum fuer Luft- und Raumfahrt) entitled *Improved Spectroscopy for Carbon Dioxide, Oxygen, and Water Vapour Satellite Measurements* for which the authors are sub-contractants. M. Birk and G. Wagner from DLR are acknowledged for fruitful discussions.

References

[1] Benner DC, Devi VM, Sung K, Brown LR, Miller CE, Payne VH, Drouin BJ, Yu S, Crawford TJ, Mantz AW, Smith MAH, Gamache RR. Line parameters including temperature dependences of air- and self-broadened line shapes of $^{12}C_{16}O_2$: 2.06-µm region. J Mol Spectrosc 2016;326:21-47. Doi:10.1016/j.jms.2016.02.012.

[2] Toth RA, Brown LR, Miller CE, Devi VM, Benner DC. Line strengths of $^{12}C^{16}O_2$: 4550–7000 cm^{-1}. J Mol Spectrosc 2006;239:221–242. Doi: 10.1016/j.jms.2006.08.001

[3] Toth RA, Brown LR, Miller CE, Devi VM, Benner DC. Self-broadened widths and shifts of $^{12}C^{16}O_2$: 4750–7000 cm^{-1}. J Mol Spectrosc 2006;239:243–271. Doi: 10.1016/j.jms.2006.08.003

[4] Toth RA, Miller CE, Devi VM, Benner DC, Brown LR. Air-broadened half width and pressure shift coefficients of $^{12}C^{16}O_2$ bands: 4750–7000 cm^{-1}. J Mol Spectrosc 2007;246:133–157. Doi: 10.1016/j.jms.2007.09.005

[5] Toth RA, Miller CE, Brown LR, Devi VM, Benner DC. Line positions and strengths of $^{16}O^{12}C^{18}O$, $^{18}O^{12}C^{18}O$ and $^{17}O^{12}C^{18}O$ between 2200 and 7000 cm^{-1}. J Mol Spectrosc 2007;243:43–61. Doi: 10.1016/j.jms.2007.03.005

[6] Toth RA, Brown LR, Miller CE, Devi VM, Benner DC. Spectroscopic database of CO_2 line parameters: 4300–7000 cm^{-1}. J Quant Spectrosc Radiat Transfer 2008;109:906–921. Doi: 10.1016/j.jqsrt.2007.12.004

[7] Suarez CB, Valero FPJ. Temperature dependence of self-broadened halfwidths of CO_2. J Quant Spectrosc Radiat Transfer 1990;43:327–334. Doi: 10.1016/0022-4073(90)90022-X

[8] Régalia-Jarlot L, Zénninari V, Parvitte B, Grossel A, Thomas X, Heyden von der P, et al. A complete study of the line intensities of four bands of CO_2 around 1.6 and 2.0 µm: a comparison between Fourier transform and diode laser measurements. J Quant Spectrosc Radiat Transfer 2006;101:325–338. Doi: 10.1016/j.jqsrt.2005.11.021

[9] Joly L, Gibert F, Grouiez B, Grossel A, Parvitte B, Durry G, Zénninari V. A complete study of CO_2 line parameters around 4845 cm^{-1} for lidar applications. J Quant Spectrosc Radiat Transfer 2008;109:426–434. Doi: 10.1016/j.jqsrt.2007.06.003

[10] Joly L, Marnas F, Gibert F, Bruneau D, Grouiez B, Flamant PH, Durry G, et al. Laser diode absorption spectroscopy for accurate CO_2 line parameters at 2 µm: consequences for space-based DIAL measurements and potential biases. Appl Opt 2009;48:5475–5483.

[11] Li JS, Durry G, Cousin J, Joly L, Parvitte B, Flamant PH, et al. Tunable diode laser measurement of pressure-induced shift coefficients of CO_2 around 2.05 µm for lidar applications. J Quant Spectrosc Radiat Transfer 2011;112:1411–1419. Doi: 10.1016/j.jqsrt.2011.01.030

[12] Li JS, Durry G, Cousin J, Joly L, Parvitte B, Zénninari V. Self-induced pressure shift and temperature dependence measurements of CO_2 at 2.05 µm with a tunable diode laser spectrometer. Spectrochim Acta A 2012;85:74–78. Doi: 10.1016/j.saa.2011.09.016

[13] Christensen LE, Spiers GD, Menzies RT, Jacob JC. Tunable laser spectroscopy of CO_2 near 2.05 µm: atmospheric retrieval biases due to neglecting line-mixing. J Quant Spectrosc Radiat Transfer 2012;113:739–748. Doi: 10.1016/j.jqsrt.2012.02.031

[14] Casa G, Wehr R, Castrillo A, Fasci E, Gianfrani L. The line shape problem in the near-infrared spectrum of self-colliding CO_2 molecules: experimental investigation and test of semiclassical models. J Chem Phys 2009;130:184306. Doi: 10.1063/1.3125965

[15] Bui TQ, Long DA, Cygan A, Sironneau VT, Hogan DW, Rupasinghe PM, Ciuryło R, Lisak D, Okumura M. Observations of Dicke narrowing and speed dependence in air-broadened CO_2 lineshapes near 2.06 µm. J Chem Phys 2014;141:174301. Doi: 10.1063/1.4900502

[16] Fleurbaey H, Yi H, Adkins EM, Fleisher AJ, Hodges JT. Cavity ring-down spectroscopy of CO_2 near λ = 2.06 µm: Accurate transition intensities for the Orbiting Carbon Observatory-2 (OCO-2) "strong band". J Quant Spectrosc Radiat Transfer 2020;252:107104. Doi: 10.1016/j.jqsrt.2020.107104.

[17] Wunch D, Toon GC, Blavier JFL, Washenfelder RA, Notholt J, Connor BJ, Griffith DWT, Sherlock V, Wennberg PO. The Total Carbon Column Observing Network. Philos T R Soc A 2011;369:2087–2112. Doi:10.1098/rsta.2010.0240.

[18] ISOGG project TechNote: WP2200: Retrieval simulations. 2022

[19] Oyafuso F, Payne VH, Drouin BJ, Devi VM, Benner DC, Sung K, Yu S, Gordon IE, Kochanov R, Tan Y, Crisp D, Mlawer EJ, Guillaume A. High accuracy absorption coefficients for the Orbiting Carbon Observatory-2 (OCO-2) mission: Validation of updated carbon dioxide cross-sections using atmospheric spectra. J Quant Spectrosc Radiat Transfer 2017;203:213-223. Doi: 10.1016/j.jqsrt.2017.06.012.

[20] Nguyen HT, Ngo NH, Tran H. Line-shape parameters and their temperature dependences predicted from molecular dynamics simulations for O_2- and air-broadened CO_2 lines. J Quant Spectrosc Radiat Transf 2020;242:106729. Doi: 10.1016/j.jqsrt.2019.106729.

[21] Hashemi R, Gordon IE, Tran H, Kochanov RV, Karlovets EV, Tan Y, Lamouroux J, Ngo NH, Rothman LS. Revising the line-shape parameters for air- and self broadened CO_2 lines toward a sub-percent accuracy level, J Quant Spectrosc Radiat Transf 2020;256:107283. Doi: 10.1016/j.jqsrt.2020.107283.
[22] Gordon IE, Rothman LS, Hargreaves RJ, Hashemi R, Karlovets EV, Skinner FM, Conway EK, Hill C, Kochanov RV, Tan Y, Wcisło P, Finenko AA, Nelson K, Bernath PF, Birk M, Boudon V, Campargue A, Chance KV, Coustenis A, Drouin BJ, Flaud J-M, Gamache RR, Hodges JT, Jacquemart D, Mlawer EJ, Nikitin AV, Perevalov VI, Rotger M, Tennyson J, Toon GC, Tran H, Tyuterev VG, Adkins EM, Baker A, Barbe A, Canè E, Császár AG, Dudaryonok A, Egorov O, Fleisher AJ, Fleurbaey H, Foltynowicz A, Furtenbacher T, Harrison JJ, Hartmann J-M, Horneman V-M, Huang X, Karman T, Karns J, Kassi S, Kleiner I, Kofman V, Kwabia–Tchana F, Lavrentieva NN, Lee TJ, Long DA, Lukashevskaya AA, Lyulin OM, Makhnev VY, Matt W, Massie ST, Melosso M, Mikhailenko SN, Mondelain D, Müller HSP, Naumenko OV, Perrin A, Polyansky OL, Raddaoui E, Raston PL, Reed ZD, Rey M, Richard C, Tóbiás R, Sadiek I, Schwenke DW, Starikova E, Sung K, Tamassia F, Tashkun SA, Vander Auwera J, Vasilenko IA, Vigasin AA, Villanueva GL, Vispoel B, Wagner G, Yachmenev A, Yurchenko SN. The HITRAN2020 molecular spectroscopic database. J Quant Spectrosc Radiat Transf 2022; 277:107949. Doi: 10.1016/j.jqsrt.2021.107949.
[23] Ma Q, Tipping RH, Boulet C. Modification of the Robert–Bonamy formalism in calculating Lorentzian half-widths and shifts. J Quant Spectrosc Radiat Transf 2007;103:588-596. Doi :10.1016/j.jqsrt.2006.08.001.
[24] Gamache RR, Lamouroux J. Predicting accurate line shape parameters for CO_2 transitions. J Quant Spectrosc Radiat Transf. 2013;130:158-171. Doi: 10.1016/j.jqsrt.2013.05.021.
[25] Hartmann J-M, Tran H, Toon GC. Influence of line mixing on the retrievals of atmospheric CO_2 from spectra in the 1.6 and 2.1 µm regions. Atmos Chem Phys 2009;9:7303–7312. Doi: 10.5194/acp-9-7303-2009
[26] Thompson DR, Benner DC, Brown LR, Crisp D, Devin VM, Jiang Y, et al. Atmospheric validation of high accuracy CO2 absorption coefficients for the OCO-2 mission. J Quant Spectrosc Radiat Transf 2012;113:2265–76. Doi :10.1016/j.jqsrt.2012.05.021
[27] https://atmos.eoc.dlr.de/isogg/about/
[28] Copernicus CO2 Monitoring Mission Requirements Document, EOP-SM/3088/YM-ym, Issue 3.0 (2020).
[29] Mondelain D, Campargue A, Fleurbaey H, Kassi S, Vasilchenko S. CRDS measurements of air-broadened lines in the 1.6 µm band of $^{12}CO_2$: Line shape parameters with their temperature dependence. J Quant Spectrosc Radiat Transf 2022;288:108267. Doi : 10.1016/j.jqsrt.2022.108267
[30] Mondelain D, Kassi S, Sala T, Romanini D, Marangoni M, Campargue A. Sub-MHz accuracy measurement of the S(2) 2–0 transition frequency of D_2 by comb-assisted cavity ring down spectroscopy. J Mol Spectrosc 2016;326:5-8. Doi:10.1016/j.jms.2016.02.008.
[31] Mondelain D, Mikhailenko SN, Karlovets EV, Béguier S, Kassi S, Campargue A. Comb-Assisted Cavity Ring Down Spectroscopy of ^{17}O enriched waterbetween 7443 and 7921 cm^{-1}. J Quant Spectrosc Radiat Transf 2017;203:206-212. Doi:10.1016/j.jqsrt.2017.03.029.
[32] Kassi S, Guessoum S, Abanto JCA, Tran H, Campargue A, Mondelain D. Temperature dependence of the collision-induced absorption band of O_2 near 1.27 µm. J Geophys Res Atm 2021;126:e2021JD034860. Doi : 10.1029/2021JD034860.
[33] Vasilchenko S, Delahaye T, Kassi S, Campargue A, Armante R, Tran H, Mondelain D. Temperature dependence of the absorption of the R(6) manifold of the $2\nu_3$ band of methane in air in support of the MERLIN mission. Submitted to JQSRT.
[34] Tran H, Ngo NH, Hartmann J-M. Efficient computation of some speed-dependent isolated line profiles. J Quant Spectrosc Radiat Transf 2013;129:199-20. Doi :10.1016/j.jqsrt.2013.06.015.
[35] Rosenkranz PK. Shape of the 5 µm oxygen band in the atmosphere. IEEE Trans Antennas Propag 1975;23:498–506.
[36] https://github.com/usnistgov/MATS. Doi:10.18434/M32200
[37] Wu H, Hu C-L, Wang J, Sun YR, Tan Y, Liu A-W, Hu S-M. A well-isolated vibrational state of CO_2 verified by near-infrared saturated spectroscopy with kHz accuracy. Phys Chem Chem Phys 2020;22:2841-2848. Doi: 10.1039/C9CP05121J
[38] Payne VH, Drouin BJ, Oyafuso F, Kuai L, Fisher BM, Sung K, Nemchick D, Crawford TJ, Smyth M, Crisp D, Adkins E, Hodges JT, Long DA, Mlawer EJ, Merrelli A, Lunny E, O'Dell CW. Absorption coefficient (ABSCO) tables for the Orbiting Carbon Observatories: Version 5.1. J Quant Spectrosc Radiat Transf 2020;255:107217. Doi : 10.1016/j.jqsrt.2020.107217.
[39] Devi VM, Benner DC, Sung K, Brown LR, Crawford TJ, Miller CE, Drouin BJ, Payne VH, Yu S, Smith MAH, Mantz AW, Gamache RR. Line parameters including temperature dependences of self- and air-broadened line shapes of $^{12}C^{16}O_2$: 1.6-µm region. J Quant Spectrosc Radiat Transf 2016;177:117-144. Doi: 10.1016/j.jqsrt.2015.12.020.

[40] Hartmann J-M. A simple empirical model for the collisional spectral shift of air-broadened CO2 lines. J Quant Spectrosc Radiat Transfer 2009;110(18):2019–26. doi:10.1016/j.jqsrt.2009.05.016
[41] Wilzewski JS, Birk M, Loos J, Wagner G. Temperature-dependence laws of absorption line shape parameters of the CO_2 ν_3 band. J Quant Spectrosc Radiat Transf 2018;206:296-305. Doi: 10.1016/j.jqsrt.2017.11.021.
[42] Ghysels M, Liu Q, Fleisher AJ, Hodges JT. A variable-temperature cavity ring-down spectrometer with application to line shape analysis of CO_2 spectra in the 1600 nm region. Appl Phys B 2017;123:124. Doi :10.1007/s00340-017-6686-y
[43] Lamouroux J, Régalia L, Thomas X, Auwera JV, Gamache R, Hartmann J-M. CO_2 line-mixing database and software update and its tests in the 2.1 µm and 4.3 µm regions. J Quant Spectrosc Radiat Transfer 2015;151:88–96. Doi:10.1016/ j.jqsrt.2014.09.017.
[44] Hartmann J-M, Boulet C, Robert D, Chapter IV - Collisional line mixing (within clusters of lines), Editor(s): J-M Hartmann, C Boulet, D Robert, Collisional Effects on Molecular Spectra (Second Edition), Elsevier, 2021, Pages 181-289. Doi : 10.1016/B978-0-12-822364-2.00004-0.
[45] Tran H, Flaud J-M, Gabard T, Hase F, von Clarmann T, Camy-Peyret C, Payan S, Hartmann J-M. Model, software and database for line-mixing effects in the ν_3 and ν_4 bands of CH_4 and tests using laboratory and planetary measurements—I: N_2 (and air) broadenings and the earth atmosphere. J Quant Spectrosc Radiat Transf 2006;101:284-305. Doi: 10.1016/j.jqsrt.2005.11.020.
[46] Kochanov RV, Gordon IE,. Rothman LS, Wcislo P, Hill C, Wilzewski JS. HITRAN Application Programming Interface (HAPI): A comprehensive approach to working with spectroscopic data. J Quant Spectrosc Radiat Transf 2016;177:15-30. Doi : 10.1016/j.jqsrt.2016.03.005